Journal Pre-proof

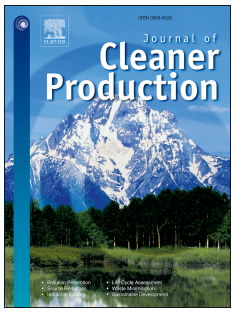

Silica-supported thiourea resin for efficient recovery of Pd(II): Batch, column and mechanism study

Zhenxiong Ye, Huidi Zhang, Xujie Chen, Lifeng Chen, Kunyapat Thummavichai, Xinpeng Wang, Toyohisa Fujita, Yuezhou Wei

PII: S0959-6526(23)02842-1

DOI: https://doi.org/10.1016/j.jclepro.2023.138684

Reference: JCLP 138684

To appear in: *Journal of Cleaner Production*

Received Date: 21 June 2023

Revised Date: 12 August 2023

Accepted Date: 3 September 2023

Please cite this article as: Ye Z, Zhang H, Chen X, Chen L, Thummavichai K, Wang X, Fujita T, Wei Y, Silica-supported thiourea resin for efficient recovery of Pd(II): Batch, column and mechanism study, *Journal of Cleaner Production* (2023), doi: https://doi.org/10.1016/j.jclepro.2023.138684.

This is a PDF file of an article that has undergone enhancements after acceptance, such as the addition of a cover page and metadata, and formatting for readability, but it is not yet the definitive version of record. This version will undergo additional copyediting, typesetting and review before it is published in its final form, but we are providing this version to give early visibility of the article. Please note that, during the production process, errors may be discovered which could affect the content, and all legal disclaimers that apply to the journal pertain.

© 2023 Published by Elsevier Ltd.

Authors' contribution:

Zhenxiong Ye: Conceptualization, Data curation, Investigation, Writing-original draft, Writing-review & editing.

Huidi Zhang: Formal analysis, Investigation.

Xujie Chen: Software, Data curation.

Lifeng Chen: Validation, Writing-review &editing

Kunyapat Thummavichai: Writing-review &editing

Xinpeng Wang: Supervision, Project administration, Funding acquisition.

Toyohisa Fujita: Resources, Visualization.

Yuezhou Wei: Supervision, Project administration.

Journal Pre-proof

Journal Pre-proof

Silica-supported thiourea resin for efficient recovery of Pd(II): Batch, column and mechanism study

Zhenxiong Ye [a,b], *Huidi Zhang* [b], *Xujie Chen* [b], *Lifeng Chen* [c], *Kunyapat Thummavichai* [d], *Xinpeng Wang* [b,*], *Toyohisa Fujita* [b], *Yuezhou Wei* [b,c].

[a] College of Chemistry and Chemical Engineering, Guangxi University, 100 Daxue East Road, Nanning 530004, PR China.

[b] State Key Laboratory of Featured Metal Materials and Life-cycle Safety for Composite Structures, School of Resources, Environment and Materials, Guangxi University, 100 Daxue East Road, Nanning 530004, PR China.

[c] School of Nuclear Science and Technology, University of South China, 28 Changsheng West Road, Hengyang 421001, PR China.

[d] Faculty of Engineering and Environment, Northumbria University, Newcastle-upon-Tyne NE1 8ST, United Kingdom.

*Corresponding author: Xinpeng Wang

Email: wangxinpeng@gxu.edu.cn

Tel:+86-0771-3224332,

Fax: +86-0771-3224332

Journal Pre-proof

Abstract: Palladium is versatile in many industrial applications due to its distinct physicochemical properties. Due to the scarcity of natural resources and the growing market demand, palladium recovery from wastes such as spent catalysts is receiving increasing attention. Here, a silica-supported thiourea resin (SiPS-TU) was prepared and applied to separate Pd(II) from spent catalysts. The SiPS-TU was fabricated through in situ polymerization and post modification method using amorphous macroporous silica as the matrix. Experimental results suggested that the optimal acidity for the adsorption process was 0.1 M under selected range, and the uptake of SiPS-TU was affected by H^+ and Cl^-. The adsorbent showed rapid sorption kinetics with an equilibrium attained in 30 min, while more than 3 h was required for the commercial D840 resin. Column tests showed that SiPS-TU had excellent dynamics separation property for Pd(II) in continuous process. Around 215 bed volumes (430 mL) of Pd(II) solution could be effective treated by the SiPS-TU bed before breakthrough at 4 mL/min, while D840 resin bed was less effective under equivalent conditions (20 mL). In view of its satisfactory adsorption performances, palladium was successfully separated from the catalyst leaching solution by SiPS-TU. XPS spectra and DFT calculations indicated that the adsorption mechanism of SiPS-TU for Pd(II) mainly involved anion exchange and coordination. In conclusion, this study provides a feasible material for palladium recovery from practical leachate.

Keywords: palladium; recovery; spent catalysts; adsorption mechanism

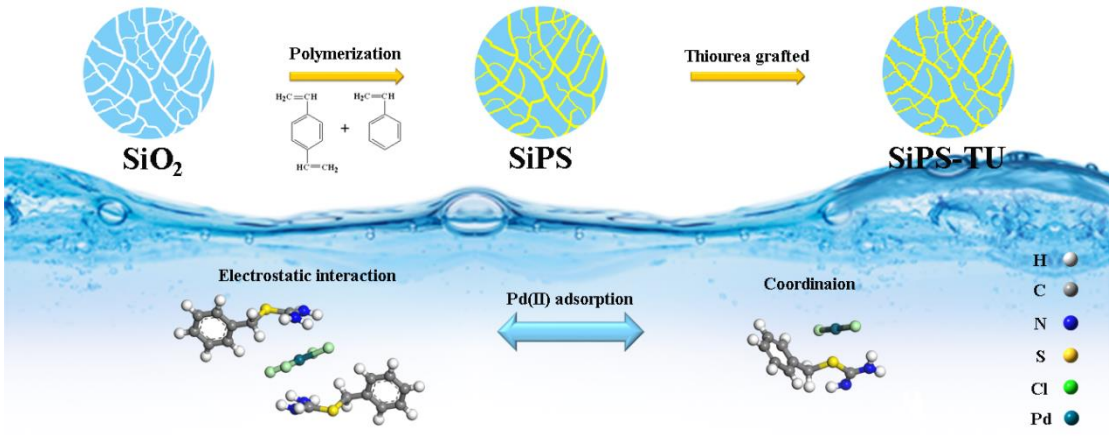

1. Introduction

Precious metals possess excellent physicochemical properties, which make them versatile materials with numerous applications in diverse industries, such as jewelry, electroplating, electronics manufacturing and catalysts production (Li et al. 2023; Lin et al. 2019; Penghui et al. 2023). Among them, palladium plays the vital role in modern catalytic systems due to the relatively low price and extraordinary catalytic ability (Bai et al. 2013; Senthil et al. 2017). The demand for palladium has soared with the rapid development of catalytic industries, while palladium resources are scarce in nature (Zhang et al. 2020). In order to mitigate the balance between tremendous consumption and limited market supply, it is imperative to explore all available resources, especially secondary resources. It has been reported that there are 20,000–30,000 tons of spent catalysts generated in China every year (Dong et al. 2015). The average content of palladium in common spent auto-catalysts is up to 150 g/t, which is far higher than that in ore (only 1–10 g/t) (Natale et al. 2017; Zhong et al. 2017). Additionally, compared with the raw ore with complex composition, the impurity of spent catalyst is much lower, which has the advantages of facile refining process and low pollution to the environment (Dong et al. 2015; Trinh et al. 2020). Therefore, recycling palladium from spent catalyst is profitable and sustainable based on the economic and environmental insight.

Generally, several hydrometallurgical steps are conducted to separate palladium from catalyst matrix. Palladium leaching is usually conducted in hydrochloric acid media with other oxidants added, such as NaOCl, HNO_3 or H_2O_2 (Li et al. 2020a; Paiva et al. 2017). Accordingly, palladium is dissolved and transferred to the leachate, mainly in form of Pd(II) and Pd(IV). To separate palladium from solutions, various techniques including chemical precipitation (Bernardis et al. 2005), adsorption (Li et al. 2020a; Petrova et al. 2019), solvent extraction (Das et al. 2014; Ngcephe et al. 2020), membrane separation (Lu et al. 2020) and electrolysis (Terrazas-Rodríguez et al. 2011) have been reported. Among them, adsorption has been acknowledged as a facile and relatively low-cost method due to its simple operability, reusability and less

waste production (Asere et al. 2019; Tang et al. 2021). Recently, many adsorption materials including metal organic frameworks (MOFs) (Lim et al. 2020), MXenes (Mu et al. 2019), nanfiber (Min et al. 2023), functionalized Amberlite XAD7 (Grad et al. 2021) and layered double hydroxides (LDHs) (Cocheci et al. 2020) have been applied to the separation of palladium. Li et al. reported a nanofiber modified by 2-Thionicitinic acid for Pd(II) adsorption, and its maximum uptake capacity reached 348.4 mg/g (Tang et al. 2021). Geng et al. synthesized amino-functionalized magnetic nanoparticles to adsorb Pd(II) with good resistance to acid and salt (Geng et al. 2020). Ciopec et al. found the dibenzo 30-crown-10 modified $MgSiO_3$ had an adsorption amount of 35.68 mg/g for palladium (Ciopec et al. 2021). Although many of these adsorbents may have the advantages in terms of kinetics, capacity or selectivity, most materials are in form of fine or even tiny powder form, which is often reported to investigate adsorption performances in batch mode. However, when dealing with large amounts of wastewater, the batch mode is restricted. There are problems in column compatibility and hydrodynamics because small particles can cause the column blocking and large pressure drops (Dong and Zhao 2018; Gao et al. 2020). This makes them unsuitable for practical applications. Therefore, the control of particle size and shape of adsorbent is significant to convert from batch test to continuous process.

Granulation of material is necessary to improve the column compatibility and hydrodynamics of sorbent. Polymeric materials have received more attention owing to the high adsorption capacity, easy shaping and excellent chemical stability (Han et al. 2022; Jia et al. 2016). For instance, Yi et al. crosslinked persimmon tannin and formaldehyde to prepare a natural resin for Pd(II) recovery from nitric acid solutions (Yi et al. 2016). The results suggested that Pd(II) separation from other metal ions can be realized in a continuous flow system. Peng et al. synthesized and reported cysteine functionalized cellulose microspheres for palladium adsorption, and the adsorbent was successfully used to recover palladium from simulated acidic waste effluent through column experiments (Peng et al. 2022). However, single polymer beads often suffer from the excessive grain size and poor pore structure, yielding the slow adsorption

rate and low separation efficiency. To overcome the drawbacks, our group has developed a series of silica-supported composites by in-situ polymerization of organic monomers in amorphous macroporous silica (Chen et al. 2016; Chen et al. 2020). The as-prepared materials possess uniform spherical shape and abundant pore structure, which have the advantages of fast mass transfer rate, excellent column compatibility and hydrodynamics (Ye et al. 2019; Chen et al. 2021). In summary, it is feasible strategy to fast and efficiently separate palladium using silica-supported functionalized polymers. On the basis of HSAB principle, palladium is classified as the soft acid, which can well interact with ligands containing N or S that belong to the soft bases (Senthil et al. 2017).

Here, silica-supported thiourea resin (SiPS-TU) was developed for palladium adsorption. The as-prepared SiPS-TU had large particle size, high specific surface area and excellent adsorption kinetics, which is able to treat palladium solution continuously through column experiments. Finally, palladium was successfully separated from the practical leaching solution using SiPS-TU. The adsorption mechanism of Pd(II) on SiPS-TU was proposed through a series of characterizations and DFT calculations. This study demonstrates a promising sorbent for the separation of palladium, and provides an efficient strategy to synthesize large-sized material used for continuous separation process.

1. Experimental

2.1 Chemicals and reagents

Amorphous macroporous silica (SiO_2) was provided by Fuji Silysia Chemical Ltd. (Japan), which was served as the skeleton to load functional polymers. The average diameter of SiO_2 is 75–150 μm, and the porosity is 69%. The styrene, divinylbenzene (m/p-mixture, 55% purity), and palladium chloride was supplied by Aladdin (Shanghai, China). The chloromethyl methyl ether was purchased from Aike Reagent (Chengdu, China). The dioxane and ethanol were procured from Macklin (Shanghai, China). The anhydrous zinc chloride was supplied by Alfa Aesar (Shanghai, China). The chemical reagents $AlCl_3{\cdot}6H_2O$, $Co(NO_3)_2{\cdot}6H_2O$, $CuCl_2$,

$FeCl_3 \cdot 6H_2O$, $Ni(NO_3)_2 \cdot 6H_2O$, $Pb(NO_3)_2$, $ZnCl_2$, and thiourea were supplied by Jinhuada Chemical Reagent (Guangzhou, China). Additionally, ultrapure water (resistivity >18.2 MΩ) was used to prepare aqueous solution. The commercial thiourea resin (D840) was obtained from Zhejiang Zhengguang Industrial Co., Ltd.

2.2 Synthesis of silica-supported thiourea chelating resin (SiPS-TU)

The SiPS-TU was synthesized via in-situ polymerization and chemical grafting methods. The relevant preparation procedure is displayed in **Scheme 1**. First, the styrene monomers and divinylbenzene were sucked into the pores of macroporous silica under high vacuum condition. The crosslinking reaction was then conducted under a nitrogen atmosphere to obtain silica-supported polystyrene (SiPS). Second, the as-prepared SiPS were reacted with excess chloromethyl methyl ether and anhydrous zinc chloride to prepare silica-supported chloromethylated polystyrene (SiPS-CH_2Cl). The detailed preparation procedures of SiPS and SiPS-CH_2Cl were described in the literatures (Wang et al. 2019b; Chen et al. 2020). Finally, SiPS-CH_2Cl (5 g) and dioxane (20 mL) were added to a flask and stirred at 298 K. Next, the excess thiourea was dissolved into ethanol, and the saturated solution (20 mL) was added to the flask. Finally, the reaction lasted for 4 h at 358 K to obtain SiPS-TU. The products were washed with water and ethanol, and vacuum-dried at 313 K.

Journal Pre-proof

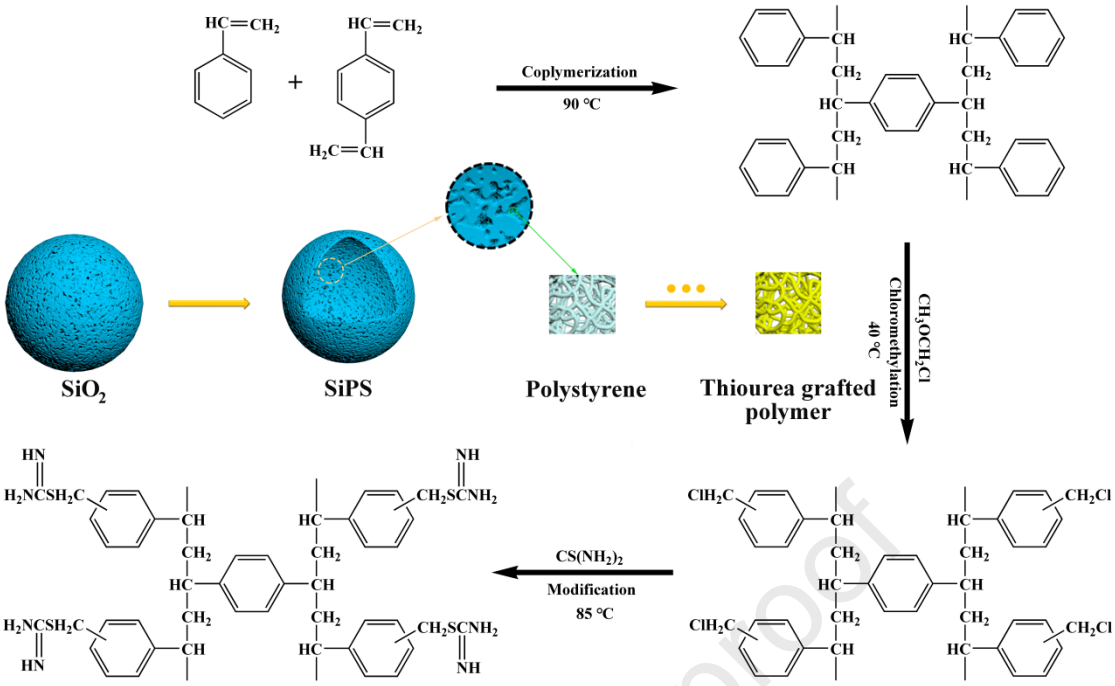

145 **Scheme 1.** Schematic illustration for silica-supported thiourea resin (SiPS-TU) synthesis.

146 2.3. Experiment

147 2.3.1. Batch experiments

148 The adsorption process was conducted at 298 K in water bath shaker with a
149 frequency of 120 rpm. 0.05 g of SiPS-TU was mixed with 20 mL of solution in the
150 experiment. The influence of acidity on the Pd(II) removal was explored with the
151 different concentration by adding hydrochloric acid, and sodium chloride was also
152 added to explore the effect of chloride. Sorption kinetics was conducted at different
153 time intervals (5 to 180 min), and Pd(II) solutions with various initial concentration
154 (50–500 mg/L) were applied to obtain the adsorption isotherms. The effect of
155 temperature (298 to 328 K) on adsorption thermodynamics was studied. An
156 inductively coupled plasma–atomic emission spectrometer (ICP-AES) was employed
157 to detect the concentration of metal ions. All the tests were repeated in triplicate with
158 the relative errors lower than 5%. The equations (Eq. (1) and Eq. (2)) were employed
159 to calculate sorption capacities (Q_e, mg/g) and distribution coefficient (K_d, mL/g):

$$Q_e = (C_0 - C_e) \times V / m \quad (1)$$

$$K_d = (C_0 - C_e) \times V / (C_e \times m) \quad (2)$$

where C_0 (mg/L) represents the initial concentration, and C_e (mg/L) is the equilibrium concentration, V (L) denotes the solution volume, and m (g) stands for the dry mass of resin.

In addition, the desorption of Pd(II) was performed with different concentrations of acidic thiourea solution. After completing desorption, the regenerated SiPS-TU was reused in the subsequent adsorption–desorption cycles.

2.3.2. Column experiments

The efficient treatment of solution in continuous mode is essential for the recovery of palladium in practical applications. Consequently, column studies were used to explore the dynamic separation performance of SiPS-TU. A glass column (diameter: 0.5 cm, bed depth: 10 cm) was used to pack the sorbents. The flow rate was adjusted using a peristaltic pump (EYELA MP2000, Japan), and the effluent was collected at predetermined intervals using an automatic fraction collector (DC-1500C, EYELA). The oral concentration level of platinum group was limited to 5 mg/L, as recommended by the EMEA (Garrett and Prasad 2004). Meanwhile, this value was adopted as the breakthrough concentration in column tests.

2.3.3. Spent catalyst leachate

In addition to palladium, some metal matrixes are also dissolved in the leaching process of spent catalyst, which makes the composition of the leachate very complicated. Thus, the applicability of SiPS-TU in real samples was further studied. Catalysts were provided by a factory in Yunnan Province, China. The leaching test was conducted with 2 M HCl and 1 M H_2O_2 solution at room temperature (Paiva et al. 2017). The filtrate was then treated with sodium oxalate solution to reduce Pd(IV) to Pd(II) for the following adsorption process. The solution acidity was adjusted to 0.1 M in the column tests. The contents of metal elements in spent catalyst and leachate are displayed in **Table 1**.

186 **Table 1** The metal contents and concentrations in spent catalyst and leachate.

Metal Element	Spent catalyst (%)	Leachate (mg/L)
Al	63.308	190
Ca	0.041	22.4
Ti	0.01	0.32
Fe	0.025	0.99
Ni	0.005	< 0.05
Ga	0.006	< 0.05
Zr	0.022	56.1
Nb	0.001	< 0.05
Pd	0.014	117.5

187 Note: The metal amounts in spent catalyst were analyzed by XRF, and the concentrations of metal
188 ions in leachate were measured using ICP-AES.

189 ## 2.4. Theoretical calculations

190 The Pd(II)-binding behavior on the SiPS-TU was investigated by the density
191 functional theory (DFT). All theoretical calculations were conducted by Gaussian 16
192 program package. Structure optimization and frequency calculation are performed
193 using the hybrid function B3LYP, where H, C, N, S, and Cl atoms use the 6-311+G(d,
194 p) basis set and Pd atom uses the LANL2DZ basis set (Arora et al. 2015). The Integral
195 Equation Formalism Polarized Continuum Model was employed to assess the effect
196 of the solvent on complex. No negative frequency occurred in the frequency
197 calculation, indicating a stable structure of the optimized complex. The optimized
198 configurations were used to calculate the adsorption energy (E_{ad}) of complex in
199 solvent, which was calculated as follows (Zhao et al. 2020; Zhang et al. 2022):

$$E_{ad} = E_{complex} - (E_{SiPS-TU} + E_{Pd(II)}) \quad (3)$$

200 where $E_{complex}$ is the total energy of complex, $E_{SiPS-TU}$ and $E_{Pd(II)}$ are the energy of
201 SiPS-TU and Pd(II), respectively.

2.5. Characterization

The relevant characterization techniques and instruments were given in the **Supporting Information**.

3. Results and discussions

3.1. Material characterization

SEM testing is employed to observe the morphology of as-prepared material. From **Fig. 1a** and **b**, SiPS-TU was composed of uniform spheres with diameters of 75–150 μm, and it possessed abundant pores on its surface (**Fig. 1c**). In the EDS photographs of SiPS-TU cross section (**Fig. 1d**), the existence of N and S elements confirmed the successful grafting of thiourea group. Moreover, palladium was homogeneously dispersed on the cross section, indicating that Pd(II) was adsorbed to the SiPS-TU. Generally, these results suggested that the functional polymer was successfully embedded into the pores of SiO_2.

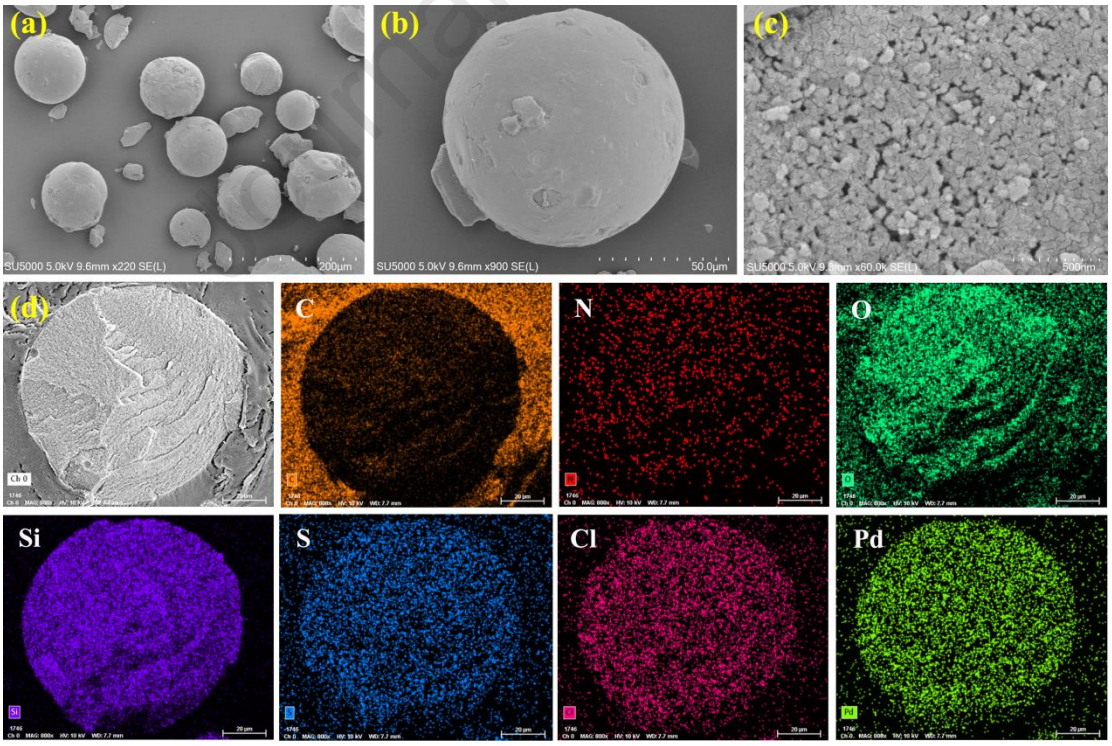

Fig. 1. SEM image of SiPS-TU magnified **(a)** 220×, **(b)** 900×, and **(c)** 60,000×. **(d)** Cross section of SiPS-TU loaded with Pd(II) and corresponding EDS mapping spectrum.

Thermal analysis is employed to estimate the organic content of material. As shown in **Fig. 2a**, there was a total weight reduction of 28.86% when the temperature ranged from 25 to 650 ℃. A slight mass loss (about 0.65%) accompanied by an endothermic process was observed before the sample was heated to 150 ℃, and it caused by the volatilization of water. A large endothermic peak appeared from 150 to 250 ℃, corresponding to a weight change of 5.57%. The decomposition of thiourea groups was primarily responsible for this mass loss stage. The weight variation of 22.64% in the temperature range of 250–650 ℃ was assigned to the oxygenolysis of polymer frameworks. In addition, the weight loss and differential thermal curve of D840 resin are shown in **Fig. 2b**. The temperature variations were basically consistent with those of the SiPS-TU, indicating the successful synthesis of thiourea functionalized polymer inside the pores of SiO_2.

Fig. 2c displays the N_2 adsorption/desorption curves of SiPS-TU and corresponding pore diameter distribution. The isotherm of SiPS-TU had an H1 hysteresis loop and belonged to type IV, implying the existence of mesopore. Almost no N_2 adsorption was observed when the relative pressure was lower than 0.8, indicating that there were few micropores in the SiPS-TU. At higher P/P_0, the capillary condensation for SiPS-TU was nearly vertical, which could be ascribed to its good pore connectivity. Moreover, most of pores were distributed in the narrow range of 25–100 nm. According to **Table 2**, the average pore size of SiPS-TU was 46.16 nm, further demonstrating its mesoporous structure. Compared with pure SiO_2, the pore volume of SiPS-TU was significantly reduced due to the presence of organic polymer. The pore volume and average pore diameter of SiPS-TU decreased after adsorption, indicating that Pd(II) was adsorbed into the pores of SiPS-TU. Additionally, compared with the D840 resin, SiPS-TU had a larger specific surface area, which was conducive to expose more active sites for fast adsorption.

To characterize the chemical composition of SiO_2 and SiPS-TU, their FT-IR spectra is shown in **Fig. 2d**. The band at 1105, 800, and 471 cm^{-1} can be ascribed to stretching and bending vibrations of Si–O, which were related to the SiO_2 matrix (Huang et al. 2020). The peaks (3440 and 1640 cm^{-1}) of adsorbed water were found in

the SiO_2 sample (Chen et al. 2019). The C−H bonds stretching vibrations (2925 cm^{-1}) could be observed in SiPS-TU, which came from aliphatic chains of the polymer (Bediako et al. 2021). There were two new bands at 1435 and 3410 cm^{-1} linked with C–N and N–H bonds, and the appearance of band at 1652 cm^{-1} was ascribed to NH_2 groups (Yun et al. 2018; Zhang et al. 2021b). Furthermore, a new band occurred at 700 cm^{-1} corresponded to the stretching vibration of C–S bond (Sharma and Rajesh 2016). These results demonstrated that thiourea groups were successfully grafted to the silica-supported polymer matrix.

Elemental analysis is performed to measure the element (C, H, N and S) content of material. The relevant results for these four elements are summarized in **Table S2**. The mass fractions for N and S were 2.925% and 2.9895%, corresponding to 2.089 and 0.934 mmol per gram of SiPS-TU, respectively. Moreover, the molar ratio of N/S (2.237) was close to the theoretical value 2 for the thiourea group.

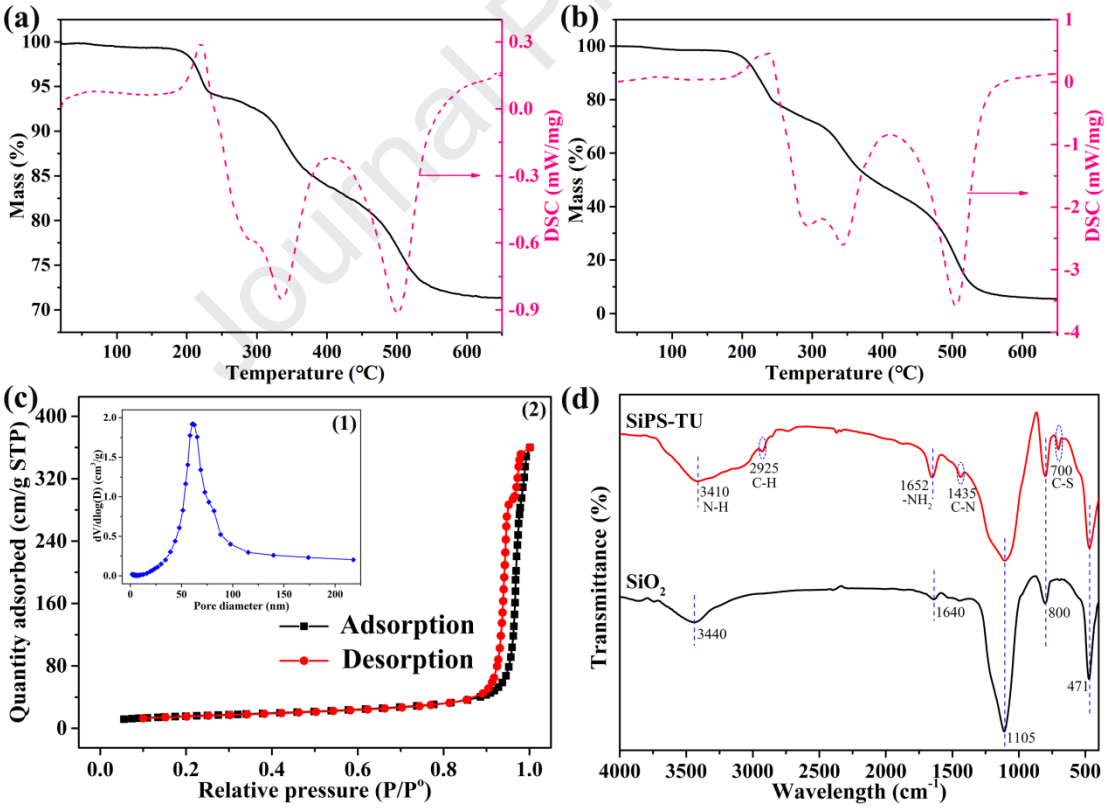

Fig.2. Thermogravimetric curves of **(a)** SiPS-TU and **(b)** D840 resin, **(c1)** Pore diameter distribution, **(c2)** N_2 adsorption/desorption isotherms, (d) FT-IR spectra.

Table 2 N_2 adsorption/desorption parameters of samples.

Sample	BET specific surface area	Average pore diameter	Pore volume
	m^2/g	nm	cm^3/g
SiPS-TU	55.39	46.16	0.53
SiPS-TU-Pd	50.15	29.18	0.32
SiO_2	68.18	77.29	0.98
D840	15.45	24.34	0.09

3.2. Batch tests

3.2.1. Influence of hydrochloric acidity and chloride

As mentioned earlier, hydrochloric acid is usually used with oxidizing agent to leach palladium. Thus, it is essential to investigate the impact of HCl on palladium sorption. **Fig. 3a** shows the adsorbed amounts of Pd(II) under different HCl concentrations. The adsorption amount of Pd(II) attained a maximum value (40.72 mg/g) at 0.1 M HCl. As the acidity increases, the Pd(II) uptake amount decreased obviously. Thermodynamic calculations suggested that the anionic chloro-complex $PdCl_4^{2-}$ (species proportion exceeded 80%) was the primary species of Pd(II) in the studied HCl systems (**Table S4**). The pH_{PZC} value for SiPS-TU is around 3.5, which means that the material will be protonated and positive charged in HCl solution (**Fig. S1b**). The positive Zeta potentials further demonstrated that the surface of SiPS-TU is positively charged, and it can interact with negatively charged $PdCl_4^{2-}$ by electrostatic attraction (**Fig. S1a**). With the increase of HCl concentration, the competitive adsorption between chloride and $PdCl_4^{2-}$ was enhanced, and thus the adsorption capacity of Pd(II) was significantly reduced.

In addition to the effect of acidity, the adsorption properties of SiPS-TU were studied under the different concentrations of chloride ions. **Fig.3b** shows the Pd(II) sorption capacity under different concentrations of NaCl. At higher concentrations of chloride ions, the poor uptake for Pd(II) was obtained. This implied that there was fierce competition between Cl^- and $PdCl_4^{2-}$ during Pd(II) adsorption, suggesting that

the interaction mechanism involved anion exchange pathway. Compared with NaCl, HCl had a greater inhibitory on Pd(II) adsorption, implying that H^+ also had adverse effect on the adsorption of Pd(II).

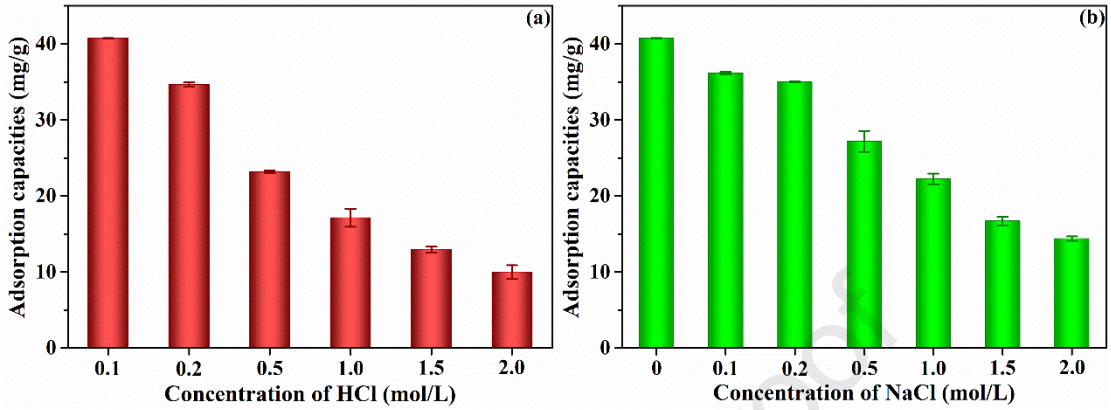

Fig. 3. Influence of **(a)** HCl and **(b)** NaCl concentrations on Pd(II) sorption (acidity: 0.1 M).

3.2.2. Sorption kinetics

To assess the impact of the reaction time, kinetics studies were performed at different time intervals. **Fig. 4a** shows that Pd(II) adsorption amount rises quickly within 5 min and approached equilibrium state at about 30 min. The kinetic curve of D840 resin climbed slowly, and it took more than 180 min to reach the equilibrium state. The results suggested that SiPS-TU had a faster sorption rate than D840 resin, and its excellent kinetics were primarily attributable to the greater specific surface area. Moreover, the sorption results were analyzed with pseudo-first-order and pseudo-second kinetic models. The fitted curves and corresponding data were displayed in **Fig. 4b** and **Table S5**. For both resins, the better fit was attained using the pseudo-second-order model, implying that chemisorption was dominated in Pd(II) sorption. Moreover, intraparticle diffusion model was employed to further elucidate the mass transfer mechanism. There are three linear parts in the sorption process of Pd(II) onto SiPS-TU (**Fig. S2**). The initial stage (I) represented the external diffusion process in which metal ions were transferred from solution to the surface of sorbent. The intrapaticle diffusion process corresponded to the second stage (II), where the metal ions diffused from the external surface into the pores of particle. The adsorption reaction reached equilibrium at the third stage (III). Three lines did not go through the

coordinate origin, indicating the rate-limiting step of Pd(II) adsorption process on the SiPS-TU included external diffusion and intrapaticle diffusion (Li et al. 2020b).

3.2.3. Sorption isotherm

Sorption isotherm is the indispensable index to evaluate the adsorption ability of adsorbents. **Fig. 4c** shows the Pd(II) adsorption isotherm of SiPS-TU at 298 K. As depicted, the uptake amounts of metal ions were positively related to their equilibrium concentrations, and no saturation was achieved. This indicated that increasing the concentration of Pd(II) can attain the higher adsorption amount. The maximum sorption amount of SiPS-TU was 75.93 mg/g when 500 mg/L of Pd(II) was provided. The related results are displayed in **Table S6**. The highest R^2 (0.999) for the Redlich–Peterson isotherm model suggested that this model provided a satisfactory description for the experimental data. The fit curve of Redlich–Peterson model was nearer to that of Freundlich model, and thus, heterogeneous multilayer adsorption was predominant in Pd(II) adsorption. Additionally, the adsorption performances of SiPS-TU and other adsorbents were compared, as shown in **Table 3**. The SiPS-TU had a relatively higher uptake amount, and showed great advantages in the adsorption rate. Thus, SiPS-TU could be used for the rapid and efficient capture of palladium.

Table 3 Comparison of the sorption properties of SiPS-TU and reported sorbents for Pd(II).

Adsorbent	Equilibrium time	Sorption capacity	HCl solution	Reference
SiO_2@GO-IIP	90 min	154.8 mg/g	pH = 3	(Li et al. 2020a)
Ch-DCMC	< 120 min	89.4 mg/g	pH = 2	(Asere et al. 2019)
HABA/PEI	> 58 h	158.57 mg/g	0.1 M	(Wang et al. 2019a)
BTU-PT Gel	> 12 h	183.04 mg/g	0.1 M	(Gurung et al. 2012)
ZrO_2-TOA	200 min	44.6 mg/g	pH = 0.3	(Trieu et al. 2020)
Pd-IIPs	60 min	38.9 mg/g	pH = 0.5	(Jiang and Kim 2013)
SIR-1	150 min	52.77 mg/g	1.0 M	(Turanov et al. 2017)
Pd-IIP-AHTB	35 min	60 mg/g	pH = 3	(Zhang et al. 2021a)
D840	> 180 min	238.83 mg/g	0.1 M	This work

SiPS-TU	**30 min**	**75.93 mg/g**	**0.1 M**	**This work**

3.2.4. Adsorption thermodynamics

The impact of temperature on Pd(II) sorption of SiPS-TU were studied at various temperatures. The linear fit of K_d versus $1/T$ and relevant parameters are displayed in **Fig. 4d** and **Table S7**. The negative value of ΔG and positive value of ΔH indicated that the Pd(II) sorption of SiPS-TU was a spontaneous and endothermic process. Consequently, a higher temperature corresponded to greater uptake capacity. Furthermore, the positive ΔS value implied that the disorder increased in the sorption of Pd(II).

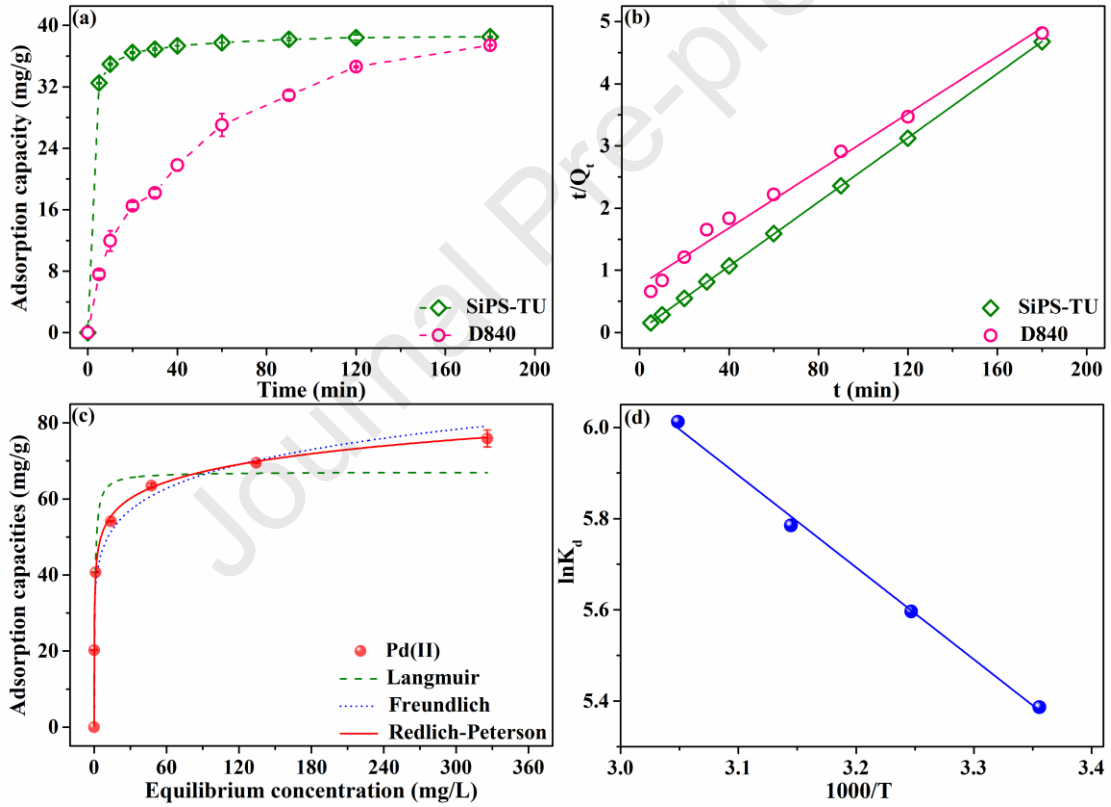

Fig. 4. (a) Sorption kinetics of Pd(II) on SiPS-TU and D840 resin, **(b)** the pseudo-second-order kinetics fitting curves, **(c)** sorption isotherm of SiPS-TU toward Pd(II), and **(d)** plot of lnK_d versus $1/T$ in linear fit.

3.2.5. Desorption and reusability

Acidic thiourea solution with different concentrations were utilized for Pd(II) elution. The enhanced thiourea concentration yielded a higher desorption efficiency,

while the increase of HCl concentration had little impact on it (**Fig. 5a**). As the concentration of thiourea rose to 0.25 M, the desorption efficiency of Pd(II) was up to 99.4%. Therefore, palladium was desorbed using 0.25 M thiourea and 0.25 M hydrochloric acid solution. Furthermore, the reusability of SiPS-TU was investigated in five adsorption–desorption runs. The Pd(II) sorption performance of SiPS-TU over five cycles was evaluated (**Fig. 5b**), and the adsorption efficiency still exceeds 90% in the fifth cycle. The results suggested that SiPS-TU possessed good reusability and showed great potential for palladium recovery.

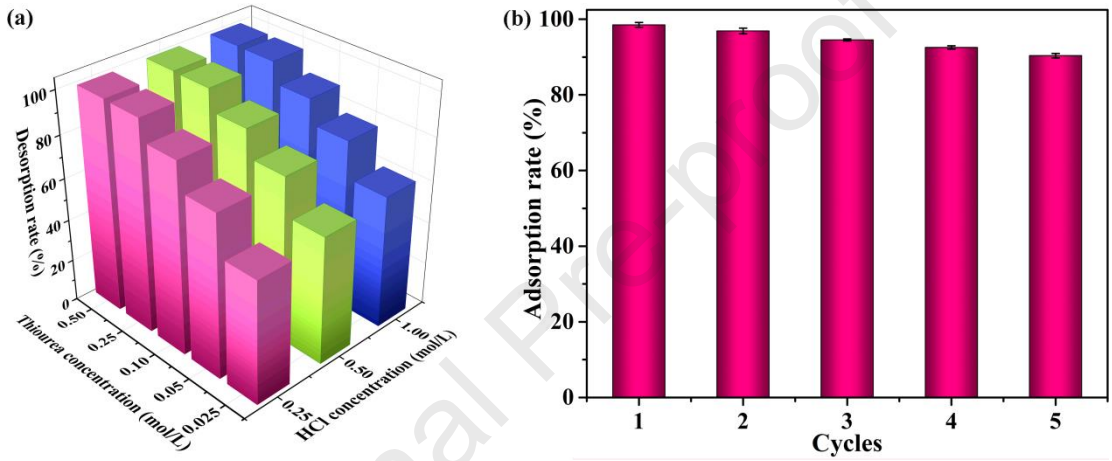

Fig. 5. (a) Influence of the concentrations of thiourea and HCl on palladium desorption, **(b)** reusability of SiPS-TU over five cycles (solution: 20 mL, Pd(II) concentration: 100 mg/L, time: 3 h).

3.3. Column tests

3.3.1. Influence of flow rate

For a dynamic adsorption system, the selection of flow rate is essential for the efficient operation of a fixed-bed column. An optimum flow rate not only ensures that the adsorbent is utilized sufficiently but also achieves faster adsorption. Consequently, the Pd(II) sorption on SiPS-TU in a column was investigated under different flow rates. Specifically, a column filled with 0.125 g of SiPS-TU was employed to dispose of 50 mL of Pd(II) solution. **Fig. 6a** displays the concentration curves of Pd(II) at various flow rates. The concentration distributions of palladium in the effluent had similar trend at flow rate less than 4 mL/min. When the flow rate was increased to 5

mL/min, a noticeable change occurred. Therefore, 4 mL/min was set as the optimal flow rate and employed for the whole column separation.

3.3.2. Dynamic sorption and elution

Both SiPS-TU and D748 resin were applied to dispose of 100 mg/L Pd(II) solution at a flow rate of 4 mL/min. **Fig. 6b** shows the Pd(II) breakthrough curves of both resins. The curve for SiPS-TU had an "S" shape with a steep concentration profile, and about 215 BV (430 mL) of solution could be treated before breakthrough. For the D840 resin bed, the concentration profile climbed relatively slowly, and breakthrough occurred after 20 BV (40 mL) of effluent, implying this resin had poor efficacy at this operating flow rate. In contrast, SiPS-TU was capable of capturing Pd(II) effectively under the same conditions, which was primarily ascribed to its fast adsorption rate. These results indicated that it was feasible to treat Pd(II) solution rapidly and efficiently by SiPS-TU.

Based on the results in batch mode, 0.25 M thiourea and 0.25 M HCl solution was used for palladium elution. **Fig. 6c** shows the corresponding elution curves for both resins. Both concentration profiles were high and narrow peaks, and the curve of SiPS-TU was steeper. When the same volume of desorption solution was used, more Pd(II) could be desorbed from SiPS-TU. As depicted in **Fig. 6d**, most of palladium was eluted by around 30 BV (60 mL) of elution solution, where the desorption efficiency reached up to 76.4% for SiPS-TU and 69.5% for D840 resin. In general, SiPS-TU can be utilized as a recyclable adsorption material for the separation of Pd(II).

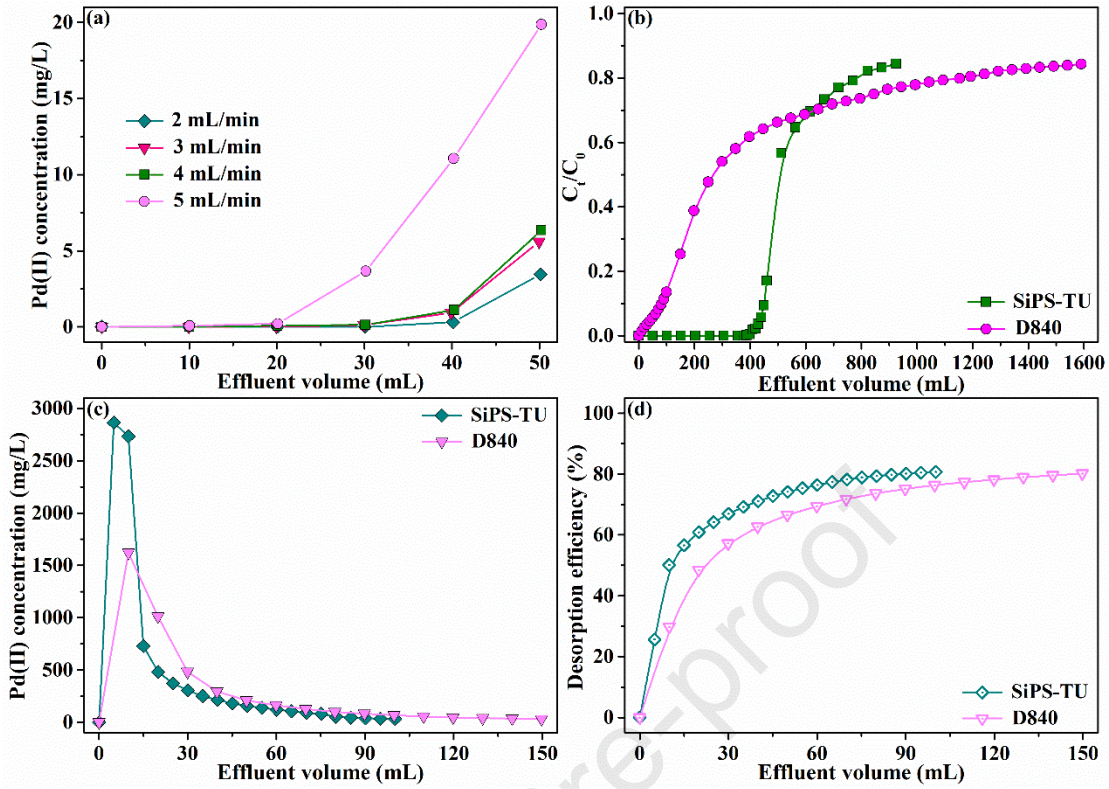

382 **Fig. 6.** Fixed-bed column tests: **(a)** influence of flow rate (concentration: 100 mg/L, acidity: 0.1
383 M), **(b)** Pd(II) breakthrough profiles (concentration: 100 mg/L, acidity: 0.1 M, flow rate: 4
384 mL/min) and **(c)** Pd(II) elution profiles of SiPS-TU and D840 resin (flow rate:1 mL/min), **(d)**
385 Pd(II) desorption efficiency of both resins.

386 3.3.3. Application to spent catalysts leachate

387 Inspired by the above experimental results, the potential of SiPS-TU to recover
388 palladium was further verified in a real leachate of spent catalyst. The breakthrough
389 profiles of Pd(II) and other metal ions are displayed in **Fig. 7a**. The coexisting metal
390 cations, including Al(III), Ca(II), Fe(III), and Ti(IV), were negligibly adsorbed on the
391 SiPS-TU bed. The curve for Zr(IV) began breakthrough when 45 BV (90 mL) of
392 leachate was disposed of, and it climbed quickly to reach the equilibrium stage.
393 However, the effluent concentration of Zr(IV) was in excess of that in the feeding
394 leachate, resulting from the chromatographic elution of Pd(II) (the adsorbed Zr(IV)
395 was exchanged with Pd(II)). A markedly retarded breakthrough curve for Pd(II)
396 adsorption from the actual leachate was obtained compared with the steep profile in
397 0.1 M HCl solution. The Pd(II) in effluent was not leakage until around 50 BV (100

mL) of leachate was treated. The effective uptake amount of Pd(II) in the practical leachate (10.68 mg/g) was lower than that in the Pd(II) solution (39.09 mg/g), which was primarily attributed to the competitive adsorption of Zr(IV) and Cl^-.

After finishing the adsorption, the palladium elution is shown in **Fig. 7b**. A high concentration Pd(II) solution containing some Zr(IV) was obtained within the first 5 BV (10 mL) of eluent. Approximately 70% desorption rate was achieved, and the average palladium concentration reached 1700 mg/L. These results indicated that about 100 mL of leachate could be effectively separated and concentrated by 1.1 g of SiPS-TU with 10 mL of eluent. For the subsequent recovery, the eluent was oxidized with H_2O_2 to obtain Pd(IV), which was precipitated with NH_4Cl to attain $(NH_4)_2PdCl_6$. After filtration, Zr(IV) remained in the filtrate and was separated from palladium. In conclusion, the usability of SiPS-TU in real leachate further demonstrated the potential of SiPS-TU to recover palladium from spent catalyst.

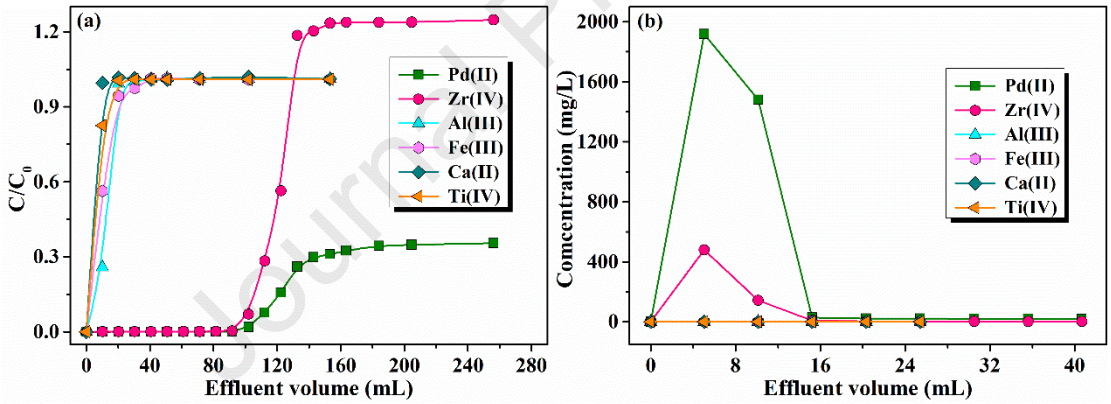

Fig. 7. Column operation for leachate: **(a)** breakthrough curves for metal ion adsorption from SiPS-TU, **(b)** elution curves for corresponding metal ions. (Flow rate: 2 mL/min for sorption and 1 mL/min for elution.)

3.4. XPS analysis

The interaction mechanism between Pd(II) and SiPS-TU was further explored by XPS spectra. In **Fig. 8a**, the XPS spectrum of SiPS-TU shows the bands of nitrogen and sulfur, demonstrating successful grafting of the thiourea group. After adsorption, two peaks located at 336.3 and 341.6 eV are assigned to Pd 3d5/2 and Pd 3d3/2 (**Fig. 8b**), indicating the successful adsorption of Pd(II) by SiPS-TU, and these results were

consistent with the above EDS analysis. Theoretical studies have found that N and S, classified as soft bases, can satisfactorily interact with palladium, classified as a soft acid. As a consequence, it is necessary to further analyze the spectra of N 1s and S 2p. As shown in **Fig. 8c**, the N 1s peaks on SiPS-TU includes two peaks at 399.3 and 400.5 eV separately corresponded to C–NH_2 and C=NH (Gladysz-Plaska et al. 2018; Liu et al. 2020). A positive shift of both peaks was observed after adsorption, which could be ascribed to the protonated of amino. In the S 2p spectrum (**Fig. 8d**), the bands at 164.4 and 165.6 eV correspond to S 2p3/2 and S 2p5/2, respectively, which should be ascribed to C–S–C bonding (Yang et al. 2018). The binding energy of S showed a negative shift after the adsorption of palladium, indicating that the sulfur atom participated in Pd(II) coordination.

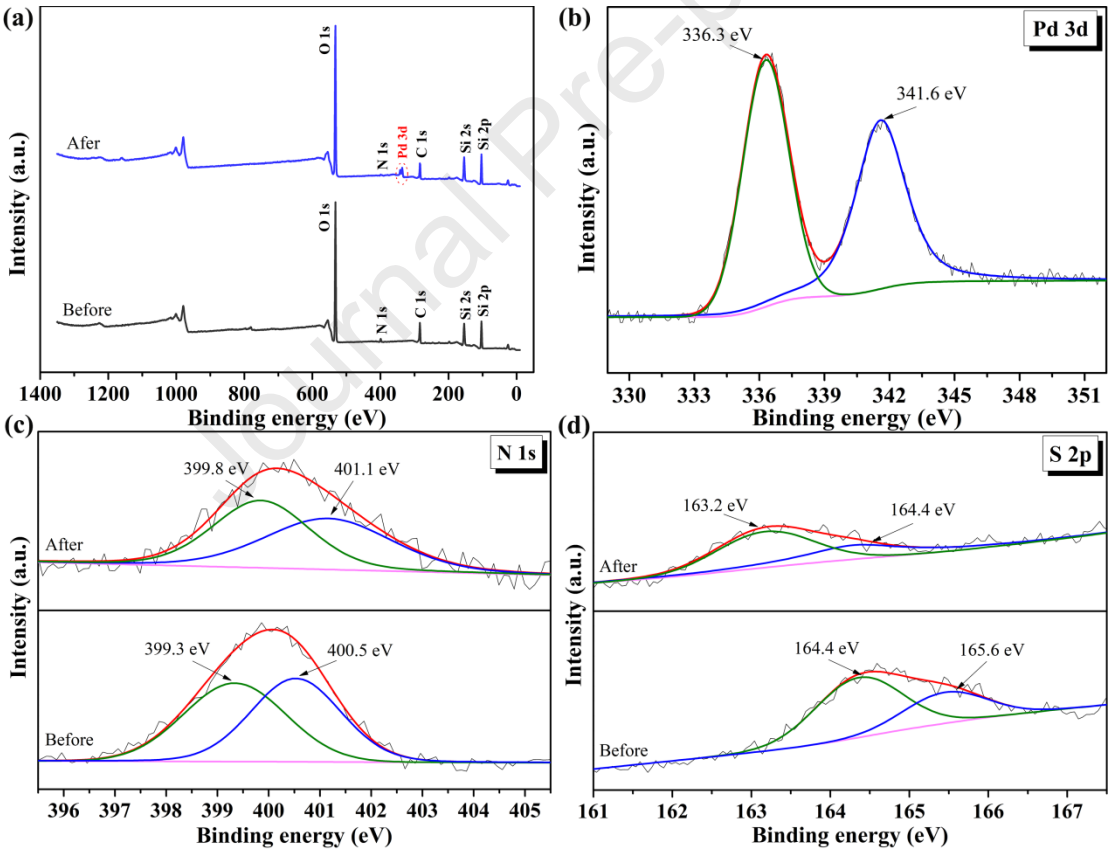

Fig. 8. XPS characterization: **(a)** The survey spectra of SiPS-TU and palladium loaded SiPS-TU (SiPS-TU-Pd), **(b)** Pd 3d spectra of SiPS-TU-Pd, **(c)** N 1s and **(d)** S 2p spectra of SiPS-TU and SiPS-TU-Pd, respectively.

3.5. DFT calculations

To understand the interaction mechanism at molecular level, DFT calculations were employed to calculate adsorption energies (E_{ad}) and bond lengths. During the optimization of geometries, a benzyl grafted with thiourea group was employed to represent the SiPS-TU for simplified molecular simulations. **Fig. 9b** shows the electrostatic potential surface of SiPS-TU, where the electron rich regions are distributed in C=NH, C–NH_2 and C–S groups. The 2p orbital of 'N' is more radially contracted, and thus is hard for metal ion to get close to bonding, whereas the lone pairs of 'S' bond easily with metal ions (Paiva et al. 2017).

The optimized geometries (**I** and **II**) f complexes together with related parameters are displayed in **Fig. 9c** and **d**. The bonding distance of Pd–S was 2.291 Å, which was shorter than that of Pd–Cl (2.320 Å). Thus there was strong interaction between Pd(II) and sulfur-containing group. The corresponding E_{ad} of complex (I) was −69.868 kcal/mol, and the results indicated Pd(II) intended to bond with the sulfur atom of SiPS-TU through monodentate coordination. In addition, the amino of SiPS-TU tended to combine H^+ and showed appreciable positive charge in the HCl system. Therefore, the negatively charged $PdCl_4^{2-}$ was prone to interact with the protonated amino driven by electrostatic attraction. The bond length of H–Cl was 2.362 Å, and the value for E_{ad} of complex (II) was −30.609 kcal/mol, implying the intensive chemical affinity. Above all, both coordination of S atom and electrostatic interaction of protonated amino are responsible for Pd(II) adsorption. The theoretical analyses were good agreement with the experimental observations.

Journal Pre-proof

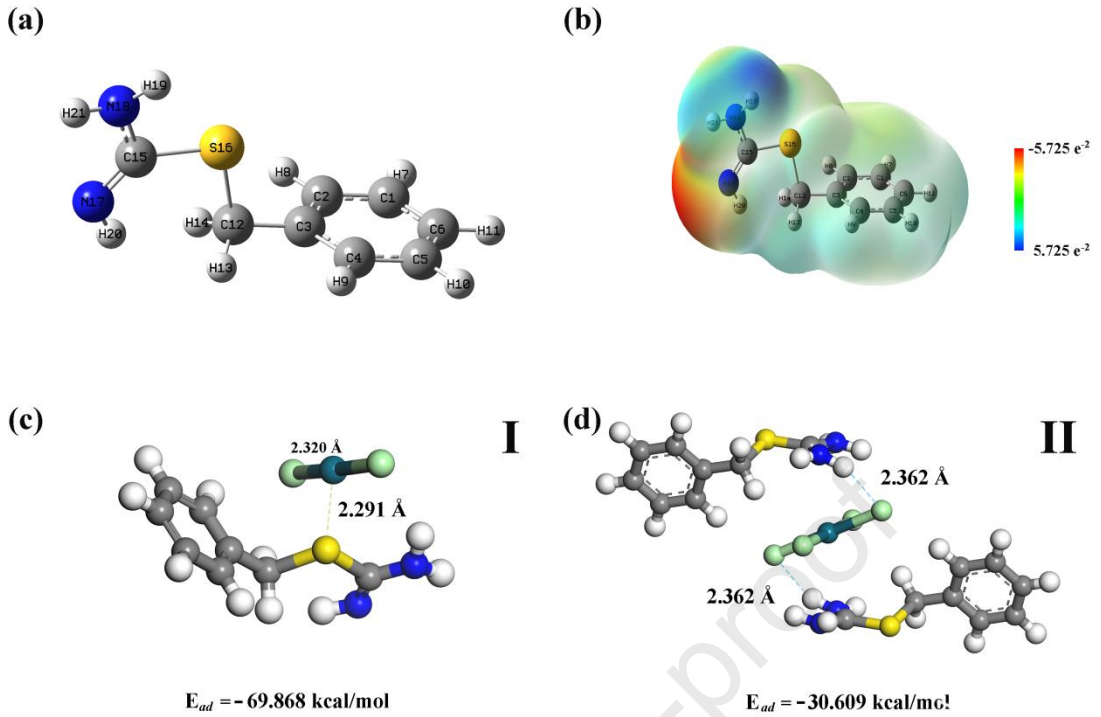

Fig. 9. DFT calculations for Pd(II) adsorption on SiPS-TU: The simplified geometry (a) and related electrostatic potential surface (b) of SiPS-TU, the optimized geometries, adsorption energy and bond length of complex I **(c)** and II **(d)**, respectively.

3.6. Mechanism study

Based on the XPS analysis and DFT calculation, there are two interaction mechanisms involved in the Pd(II) adsorption process, including anion exchange and monodentate coordination (**Scheme 2a** and **b**). To assess the proportion of adsorption through coordination relative to the total adsorption (set as k), we assumed the adsorption reaction occurred according to **Scheme 2c**. The corresponding equilibrium constant (K_p) was calculated as follows:

$$K_p = [C_A] \cdot [C_{Cl^-}]^{2k} [C_{H^+}]^k \Big/ \left([C_S]^{2-k} [C_{PdCl_4^{2-}}] \right) \quad (11)$$

where C_A and C_S represent the Pd(II) adsorption amount at equilibrium (i.e., Q_e) and the content of thiourea groups of SiPS-TU (0.934 mmol g^{-1}, **Table S1**), respectively. Subsequently, Eq. (11) was simplified in conjunction with Eq. (2) to obtain the following equation:

$$K_p = K_d \cdot \left[C_{Cl^-}\right]^{2k} \cdot \left[C_{H^+}\right]^{k} \Big/ \left(1000 \times [C_S]^{2-k}\right) \quad (12)$$

where the solution acidity is fixed at 0.1 M. Eq.(12) can be transformed to the linear form:

$$\lg K_d = -2k \times \lg C_{Cl^-} + b \quad (13)$$

where b is a constant associated with k. In view of the limited amounts of Cl^- released from the adsorption reaction and high initial concentration of Cl^- existed in aqueous phase, the Cl^- concentration can be considered as a constant value. Based on the results of the influence of chloride on the uptake amount, **Fig. 10** shows the linear fit plots of logarithm K_d versus logarithm chloride concentration. The fitting parameters indicated that the coordination behavior contributed to 40.35% of Pd(II) adsorption.

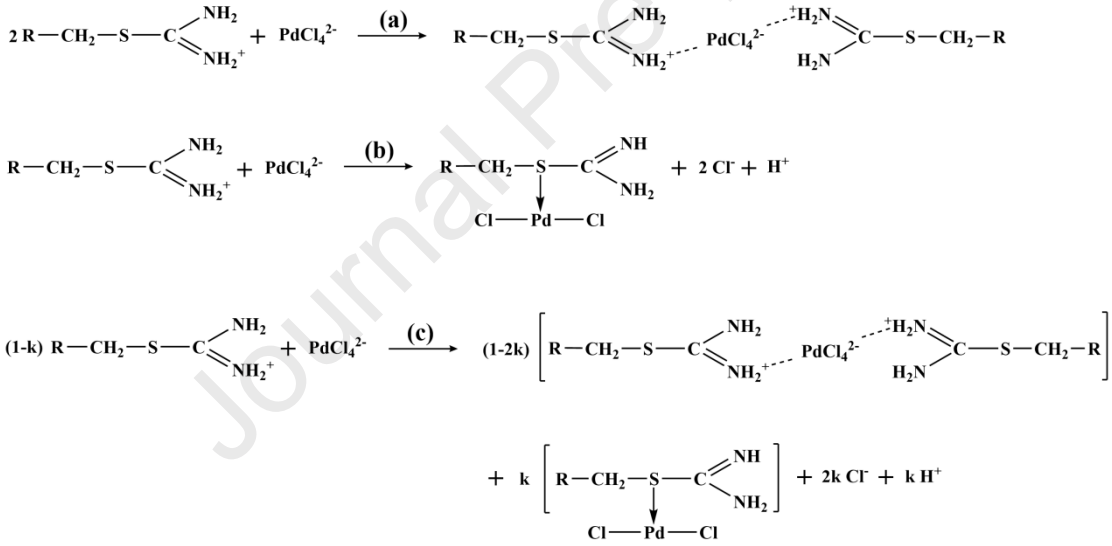

Scheme 2. Pd(II) and thiourea group adsorption pathways: **(a)** anion exchange, **(b)** coordination and **(c)** anion exchange and coordination.

Journal Pre-proof

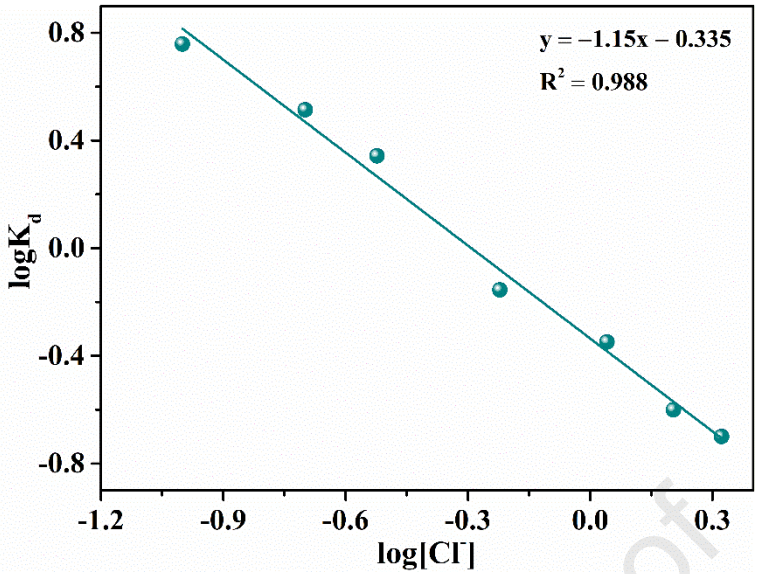

Fig. 10. Plot of K_d versus chloride concentration in linear fit.

4. Conclusion

A silica-supported thiourea resin (SiPS-TU) was developed and reported for the separation of palladium. Batch experiment results indicated that the adsorption equilibrium of SiPS-TU reached within 30 min, and it was 6-fold faster than D840 resin. The sorption behavior of SiPS-TU can be satisfactorily fitted with the pseudo-second-order kinetics and Redlich–Peterson isotherm models. Furthermore, column experiments suggested that SiPS-TU could rapidly and effectively capture Pd(II), while D840 resin bed was breakthrough quickly. This material was further utilized to separate Pd(II) from real leachate, which demonstrated the practicality of SiPS-TU. The interaction mechanism between Pd(II) and SiPS-TU involved coordination and anion exchange. Moreover, further study showed that 40.35% of the adsorption was caused by coordination behavior. In summary, this study demonstrates that the SiPS-TU is excellent sorbent for palladium separation, and offers a promising method for the preparation large-sized porous composite.

Acknowledgements

This work was supported by the Science and Technology Major Project of Guangxi [grant No.AAA17204100] and the National Natural Science Foundation of

China [grant No.21866007].

Declaration of Competing Interest

The authors declare that they have no known competing financial interests or personal relationships that could have appeared to influence the work reported in this paper.

Appendix A. Supporting information

References

Arora, J.S., Joshi, U., Gaikar, V.G., Ali, S.M., 2015. Experimental and DFT studies for selective separation of Sb(III) and Sb(V) from mixtures with Zr(IV)/Co(II) using thiourea grafted polystyrene adsorbent. RSC Adv. 5, 71393–71401. https://doi.org/10.1039/c5ra11107b.

Asere, T.G., Mincke, S., Folens, K., Bussche, F.V., Lapeire, L., Verbeken, K., Voort, P.V.D., Tessema, D.A., Laing, G.D., Stevens, C.V., 2019. Dialdehyde carboxymethyl cellulose cross-linked chitosan for the recovery of palladium and platinum from aqueous solution. React. Funct. Polym. 141, 145–154. https://doi.org/10.1016/j.reactfunctpolym.2019.05.008.

Bai, F., Ye, G., Chen, G., Wei, J., Wang, J., Chen, J., 2013. Highly selective recovery of palladium by a new silica-based adsorbent functionalized with macrocyclic ligand. Sep. Purif. Technol. 106, 38–46. https://doi.org/10.1016/j.seppur.2012.12.021.

Bediako, J.K., Choi, J.W., Song, M.H., Lim, C.R., Yun, Y.S., 2021. Self-coagulating polyelectrolyte complexes for target-tunable adsorption and separation of metal ions. J. Hazard. Mater. 401, 123352. https://doi.org/10.1016/j.jhazmat.2020.123352.

Bernardis, F.L., Grant, R.A., Sherrington, D.C., 2005. A review of methods of separation of the platinum-group metals through their chloro-complexes. React. Funct. Polym. 65, 205–217. https://doi.org/10.1016/j.reactfunctpolym.2005.05.011.

Chen, L., Zhang, J., Huang, Y., Peng, C., Chen, Y., Lu, L., Wang, X., Wei, Y., 2021. An anion exchange pretreatment method for the determination of low-level uranium in the environmental water samples. J. Environ. Radioact. 237, 106699. https://doi.org/10.1016/j.jenvrad.2021.106699.

Chen, L., Yin, X., Yu, Q., Lu, S., Meng, F., Ning, S., Wang, X., Wei, Y., 2019. Rapid and selective capture of perrhenate anion from simulated groundwater by a mesoporous silica-supported anion exchanger. Microporous Mesoporous Mater. 274, 155–162. https://doi.org/10.1016/j.micromeso.2018.07.029.

Chen, L., Zhang, J., He, X., Liu, M., Wei, Q., Wang, X., Wei, Y., 2020. Fast recovery of lead from hydrochloric acid via a novel silica-supported anion exchange resin for the determination of ^{210}Pb in environmental samples. Chem. Eng. J. 396, 125300. https://doi.org/10.1016/j.cej.2020.125300.

Chen, Y., Wei, Y., He, L., Tang, F., 2016. Separation of thorium and uranium in nitric acid solution using silica based anion exchange resin. J. Chromatogr. A 1466, 37–41. http://dx.doi.org/10.1016/j.chroma.2016.09.010.

Ciopec, M., Grad, O., Negrea, A., Duteanu, N., Negrea, P., Paul, C., Ianăși, C., Mosoarca, G., Vancea, C., 2021. A New Perspective on Adsorbent Materials Based Impregnated $MgSiO_3$ with Crown Ethers for Palladium Recovery. Int. J. Mol. Sci. 22, 10718. https://doi.org/10.3390/ijms221910718.

Cocheci, L., Lupa, L., Ţolea, N. S., Muntean, C., Negrea, P., 2020. Sequential use of ionic liquid functionalized Zn-Al layered double hydroxide as adsorbent and photocatalyst. Sep. Purif. Technol. 250, 117104. https://doi.org/10.1016/j.seppur.2020.117104.

Das, A., Ruhela, R., Singh, A.K., Hubli, R.C., 2014. Evaluation of novel ligand dithiodiglycolamide (DTDGA) for separation and recovery of palladium from simulated spent catalyst dissolver solution. Sep. Purif. Technol. 125, 151–155. https://doi.org/10.1016/j.seppur.2014.01.001.

Dong, H., Zhao, J., Chen, J., Wu, Y., Li, B., 2015. Recovery of platinum group metals from spent catalysts: A review. Int. J. Miner. Process. 145: 108–113. https://doi.org/10.1016/j.minpro.2015.06.009.

Dong, Z., Zhao, L., 2018. Covalently bonded ionic liquid onto cellulose for fast adsorption and efficient separation of Cr(VI): Batch, column and mechanism investigation. Carbohydr. Polym. 189, 190–197. https://doi.org/10.1016/j.carbpol.2018.02.038.

Gao, X., Liu, J., Li M., Guo C., Long H., Zhang, Y., Xin, L., 2020. Mechanistic study of selective adsorption and reduction of Au (III) to gold nanoparticles by ion-imprinted porous alginate

microspheres, Chem. Eng. J. 385, 123897. https://doi.org/10.1016/j.cej.2019.123897.

Garrett, C.E., Prasad, K., 2004. The Art of Meeting Palladium Specifications in Active Pharmaceutical Ingredients Produced by Pd-Catalyzed Reactions. Adv. Synth. Catal. 346, 889–900. https://doi.org/10.1002/adsc.200404071.

Geng, Y., Li, J., Lu, W., Wang, N., Xiang, Z., Yang, Y., 2020. Au(III), Pd(II) and Pt(IV) adsorption on amino-functionalized magnetic sorbents: Behaviors and cycling separation routines. Chem. Eng. J. 381, 122627. https://doi.org/10.1016/j.cej.2019.122627.

Gladysz-Plaska, A., Majdan, M., Tarasiuk, B., Sternik, D., Grabias, E., 2018. The use of halloysite functionalized with isothiouronium salts as an organic/inorganic hybrid adsorbent for uranium(VI) ions removal. J. Hazard. Mater. 354, 133–144. https://doi.org/10.1016/j.jhazmat.2018.03.057.

Grad, O., Ciopec, M., Negrea, A., Duteanu, N., Negrea, P., Vodă, R., 2021. Evaluation of Performance of Functionalized Amberlite XAD7 with Dibenzo-18-Crown Ether-6 for Palladium Recovery. Materials 14, 1003. https://doi.org/10.3390/ ma14041003.

Gurung, M., Adhikari, B.B., Kawakita, H., Ohto, K., Inoue, K., Alam, S., 2012. Selective Recovery of Precious Metals from Acidic Leach Liquor of Circuit Boards of Spent Mobile Phones Using Chemically Modified Persimmon Tannin Gel. Ind. Eng. Chem. Res. 51, 11901−11913. https://doi.org/10.1021/ie3009023.

Han, S., Zhou, X., Xie, H., Wang, X., Yang, L., Wang, H., Hao, C.,. 2022. Chitosan-based composite microspheres for treatment of hexavalent chromium and EBBR from aqueous solution. Chemosphere 305, 135486. https://doi.org/10.1016/j.chemosphere.2022.135486.

Huang, X., Ye, Z., Chen, L., Chen, X., Liu, C., Yin, Y., Wang, X., Wei, Y., 2020. Removal of V(V) From Solution Using a Silica-Supported Primary Amine Resin: Batch Studies, Experimental Analysis, and Mathematical Modeling. Molecules 25, 1448. https://doi.org/10.3390/molecules25061448.

Jia, X., Gong, D., Wang, J., Huang, F., Duan, T., Zhang, X., 2016. Arsenic speciation in environmental waters by a new specific phosphine modified polymer microsphere preconcentration and HPLC-ICP-MS determination. Talanta 160, 437–443. http://dx.doi.org/10.1016/j.talanta.2016.07.050.

Jiang, Y., Kim, D., 2013. Synthesis and selective adsorption behavior of Pd(II)-imprinted porous

polymer particles. Chem. Eng. J. 232, 503–509. https://doi.org/10.1016/j.cej.2013.08.008.

Li, M., Tang, S., Zhao, Z., Meng, X., Gao, F., Jiang, S., Chen, Y., Feng, J., Feng, C., 2020. A novel nanocomposite based silica gel/graphene oxide for the selective separation and recovery of palladium from a spent industrial catalyst. Chem. Eng. J. 386, 123947. https://doi.org/10.1016/j.cej.2019.123947.

Li, M., Yao, Z., Chen, Y., Li, D., Shao, J., Dong, H., Meng, Z., Yang, L., Ren, W., Luo, X., Shao, P., 2023. Potential-dependent selectivity for the efficient capture of gold from E-waste acid leachate using sulfhydryl-functionalized carbon. Sci. Bull. 68, 1095–1099. https://doi.org/10.1016/j.scib.2023.05.002.

Li, W., Liu, Y., Bai, Y., Wang, J., Pang, H., 2020b. Anchoring ZIF-67 particles on amidoximerized polyacrylonitrile fibers for radionuclide sequestration in wastewater and seawater. J. Hazard. Mater. 395, 122692. https://doi.org/10.1016/j.jhazmat.2020.122692.

Lim, C.-R., Lin, S., Yun, Y.-S., 2020. Highly efficient and acid-resistant metal-organic frameworks of MIL-101(Cr)-NH_2 for Pd(II) and Pt(IV) recovery from acidic solutions: Adsorption experiments, spectroscopic analyses, and theoretical computations. J. Hazard. Mater. 387, 121689. https://doi.org/10.1016/j.jhazmat.2019.121689.

Lin, S., Zhao, Y., Bediako, J.K., Cho, C.-W., Sarkar, A.K., Lim, C.-R., Yun, Y.-S., 2019. Structure-controlled recovery of palladium(II) from acidic aqueous solution using metal-organic frameworks of MOF-802, UiO-66 and MOF-808. Chem. Eng. J. 362, 280–286. https://doi.org/10.1016/j.cej.2019.01.044.

Liu, P., Wang, X., Tian, L., He, B., Lv, X., Li, X., Wang, C., Song, L., 2020. Adsorption of silver ion from the aqueous solution using a polyvinylidene fluoride functional membrane bearing thiourea groups. J. Water Process Eng. 34, 101184. https://doi.org/10.1016/j.jwpe.2020.101184.

Lu, J., Qin, Y., Yu, C., Lin, X., Meng, M., Yan, Y., Fan, H., Wu, Y., Li, C., 2020. Stable, regenerable and 3D macroporous Pd (II)-imprinted membranes for efficient treatment of electroplating wastewater. Sep. Purif. Technol. 235, 116220. https://doi.org/10.1016/j.seppur.2019.116220.

Li, M., Wang, M., Zhang, L., Fan, Y., Xu, L., Ma, Z., Wen, Z., Wang, H., Cheng, N., 2023. Adsorption of Pd(II) ions by electrospun fibers with effective adsorption sites constructed by

N, O atoms with a particular spatial configuration: Mechanism and practical applications. J. Hazard. Mater. 458, 132014. https://doi.org/10.1016/j.jhazmat.2023.132014.

Mu, W., Du, S., Li, X., Yu, Q., Wei, H., Yang, Y., Peng, S., 2019. Removal of radioactive palladium based on novel 2D titanium carbides. Chem. Eng. J. 358, 283–290. https://doi.org/10.1016/j.cej.2018.10.010.

Natale, F.D., Orefice, M., Motta, F.L., Erto, A., Lancia, A., 2017. Unveiling the potentialities of activated carbon in recovering palladium from model leaching solutions. Sep. Purif. Technol. 174, 183–193. https://doi.org/10.1016/j.seppur.2016.10.022.

Ngcephe, A.M., Sinha, M.K., Purcell, W., 2020. Solvent extraction and separation of palladium from platinum group elements: Synthesis and characterization of 2-mercaptopyridine N-oxide-palladium (II) complex. J. Mol. Struct. 1199, 127009. https://doi.org/10.1016/j.molstruc.2019.127009.

Paiva, A.P., Ortet, O., Carvalho, G.I., Nogueira, C.A., 2017. Recovery of palladium from a spent industrial catalyst through leaching and solvent extraction. Hydrometallurgy 171, 394–401. https://doi.org/10.1016/j.hydromet.2017.06.014.

Peng, L., Zhang, M., Dong, Z., Qi, W., Zhai, M., Zhao, L., 2022. Efficient and selective adsorption of Pd(II) by amino acid-functionalized cellulose microspheres and their applications in palladium recovery from PCBs leaching solution. Sep. Purif. Technol. 301, 122037. https://doi.org/10.1016/j.seppur.2022.122037.

Shao, P., Chang, Z., Li, M., Lu, X,, Jiang, W., Zhang, K., Luo, X., Yang, L., 2023. Mixed-valence molybdenum oxide as a recyclable sorbent for silver removal and recovery from wastewater. Nat. Commun. 14, 1365. https://doi.org/10.1038/s41467-023-37143-2.

Petrova, Y.S., Pestov, A.V., Kapitanova, E.I., Usoltseva, M.K., Neudachina, L.K., 2019. High-selective recovery of palladium by the N-(2-sulfoethyl)chitosan-based sorbent from the Pt(IV)-Pd(II) binary solution in a fixed-bed column. Sep. Purif. Technol. 213, 78–87. https://doi.org/10.1016/j.seppur.2018.12.025.

Senthil, K., Akiba, U., Fujiwara, K., Hamada, F., Kondo, Y., 2017. New Heterocyclic Dithioether Ligands for Highly Selective Separation and Recovery of Pd(II) from Acidic Leach Liquors of Spent Automobile Catalyst. Ind. Eng. Chem. Res. 56, 1036–1047. https://doi.org/10.1021/acs.iecr.6b03874.

Sharma, S., Rajesh, N., 2016. Augmenting the adsorption of palladium from spent catalyst using a thiazole ligand tethered on an amine functionalized polymeric resin. Chem. Eng. J. 283, 999–1008. https://doi.org/10.1016/j.cej.2015.08.061.

Tang, J., Zhao, J., Wang, S., Zhang, L., Zhao, M., Huang, Z., Hu, Y., 2021. Pre-modification strategy to prepare a novel Zr-based MOF for selective adsorption of Palladium(II) from solution. Chem. Eng. J. 407, 127223. https://doi.org/10.1016/j.cej.2020.127223.

Terrazas-Rodríguez, J.E., Gutiérrez-Granados, S., Alatorre-Ordaz, M.A., León, C.P.d., Walsh, F.C., 2011. A comparison of the electrochemical recovery of palladium using a parallel flat plate flow-by reactor and a rotating cylinder electrode reactor. Electrochim. Acta 56, 9357–9363. https://doi.org/10.1016/j.electacta.2011.08.021.

Trieu, Q.A., Pellet-Rostaing, S., Arrachart, G., Traore, Y., Kimbel, S., Daniele, S., 2020. Interfacial study of surface-modified ZrO_2 nanoparticles with thioctic acid for the selective recovery of palladium and gold from electronic industrial wastewater. Sep. Purif. Technol. 237, 116353. https://doi.org/10.1016/j.seppur.2019.116353.

Trinh, H. B., Lee, J.-c., Suh, Y.-j., Lee, J., 2020. A review on the recycling processes of spent auto-catalysts: Towards the development of sustainable metallurgy. Waste Manage. 114, 148–165. https://doi.org/10.1016/j.wasman.2020.06.030.

Turanov, A.N., Karandashev, V.K., Artyushin, O.I., Sharova, E.V., Genkina, G.K., 2017. Adsorption of palladium(II) from hydrochloric acid solutions using polymeric resins impregnated with novel N-substituted 2-(diphenylthiophosphoryl)acetamides. Sep. Purif. Technol. 187, 355–364. https://doi.org/10.1016/j.seppur.2017.06.068.

Wang, S., Vincent, T., Faur, C., Rodríguez-Castellónc, E., Guibal, E., 2019a. A new method for incorporating polyethyleneimine (PEI) in algal beads: High stability as sorbent for palladium recovery and supported catalyst for nitrophenol hydrogenation. Mater. Chem. Phys. 221, 144–155. https://doi.org/10.1016/j.matchemphys.2018.09.021.

Wang, X., Ye, Z., Chen, L., Zheng, Q., Liu, C., Ning, S., Khayambashic, A., Wei, Y., 2019b. Microporous silica-supported cation exchanger with superior dimensional stability and outstanding exchange kinetics, and its application in element removal and enrichment. React. Funct. Polym. 142, 87–95. https://doi.org/10.1016/j.reactfunctpolym.2019.06.007.

Yang, J., Gong, D., Li, G., Zeng, G., Wang, Q., Zhang, Y., Liu, G., Wu, P., Vovk, E., Peng, Z.,

675 Zhou, X., Yang, Y., Liu, Z., Sun, Y., 2018. Self-Assembly of Thiourea-Crosslinked Graphene
676 Oxide Framework Membranes toward Separation of Small Molecules. Adv. Mater. 30,
677 1705775. https://doi.org/10.1002/adma.201705775.
678 Ye, Z., Yin, X., Chen, L., He, X., Lin, Z., Liu, C., Ning, S., Wang, X., Wei, Y., 2019. An integrated
679 process for removal and recovery of Cr(VI) from electroplating wastewater by ion exchange
680 and reduction–precipitation based on a silica-supported pyridine resin. J. Cleaner Prod.
681 236, 117631. https://doi.org/10.1016/j.jclepro.2019.117631.
682 Yi, Q., Fan, R., Xie, F., Zhang, Q., Luo, Z., 2016. Recovery of Palladium(II) from nitric acid
683 medium using a natural resin prepared from persimmon dropped fruits residues. J. Taiwan Inst.
684 Chem. Eng. 61, 299–305. http://dx.doi.org/10.1016/j.jtice.2016.01.009.
685 Yun, J.-I., Bhattarai, S., Yun, Y.-S., Lee, Y.-S., 2018. Synthesis of thiourea-immobilized
686 polystyrene nanoparticles and their sorption behavior with respect to silver ions in aqueous
687 phase. J. Hazard. Mater. 344, 398–407. https://doi.org/10.1016/j.jhazmat.2017.10.050.
688 Zhang, H., Li, C., Chen, X., Fu, H., Chen, Y., Ning, S., Fujita, T., Wei, Y., Wang, X., 2022.
689 Layered ammonium vanadate nanobelt as efficient adsorbents for removal of Sr^{2+} and Cs^{+}
690 from contaminated water. J. Colloid Interface Sci. 615, 110–123.
691 https://doi.org/10.1016/j.jcis.2022.01.164.
692 Zhang, K., Chang, Z., Luo, X., Yang, L., Pei, J, Luo, S., 2021a. Specific spatial transfer $PdCl_4^{2-}$ to
693 [X-Pd-Y] by strong coordination interaction in a 3D palladium ion-imprinted polymer with
694 footprint cavity. Chem.l Eng. J. 405, 126613. https://doi.org/10.1016/j.cej.2020.126613.
695 Zhang, L., Song, Q., Liu, Y., Xu, Z., 2020. An integrated capture of copper scrap and
696 electrodeposition process to enrich and prepare pure palladium for recycling of spent catalyst
697 from automobile. Waste Manag. 108, 172–182. https://doi.org/10.1016/j.wasman.2020.04.013.
698 Zhang, M., Liu, Y., Zhao, H., Tao, J., Geng, N., Li, W., Zhai, Y., 2021b. Pd Anchored on a Phytic
699 Acid/Thiourea Polymer as a Highly Active and Stable Catalyst for the Reduction of Nitroarene.
700 ACS Appl. Mater. Interfaces 13, 19904–19914. https://doi.org/10.1021/acsami.0c23007.
701 Zhao, M., Huang, Z., Wang, S., Zhang, L., Wang, C., 2020. Experimental and DFT study on the
702 selective adsorption mechanism of Au(III) using amidinothiourea-functionalized UiO-66-NH_2.
703 Microporous Mesoporous Mater. 294, 109905.
704 https://doi.org/10.1016/j.micromeso.2019.109905.

Zhong, L., Zhang, J., Zhang, Q., Chen, M., Huang, Z., 2017. Novel poly(aniline-co-3-amino-4-methoxybenzoic acid) copolymer for the separation and recovery of Pd(ii) from the leaching liquor of automotive catalysts. RSC Adv. 7, 39244–39257. https://doi.org/10.1039/c7ra06404g.

Journal Pre-proof

Journal Pre-proof

Highlights:

1. The silica-supported thiourea resin exhibited fast adsorption kinetics.
2. The prepared material had excellent dynamic adsorption performances.
3. Both anion exchange and coordination participated in the Pd(II) adsorption.
4. The composite was able to efficiently separate Pd(II) from spent catalysts.

Journal Pre-proof

Journal Pre-proof

Declaration of Competing Interest

The authors declare that they have no known competing financial interests or personal relationships that could have appeared to influence the work reported in this paper.

Journal Pre-proof